Neuroprotective Effects and Changes in Intestinal Flora with the Huc-Mscs Treatment in LPS-Induced Inflammation Mouse Models

*Yanjie Yang[1,2#]; Tong Lei[1,2#]; Hongwu Du[1,2]**

[1]*School of Chemistry and Biological Engineering, University of Science and Technology Beijing, Beijing, 100083, China.*

[2]*Daxing Research Institute, University of Science and Technology Beijing, Beijing, 100083, China.*

*Corresponding Author(s): Hongwu Du

School of Chemistry and Biological Engineering, University of Science and Technology, 112 Lab, Lihua BLDG, No. 30 Xueyuan Road, Haidian District, Beijing 100083 China.

Email: hwdu93@126.com

\#   These authors contributed equally to this work

Keywords: Neuroinflammation; Human Umbilical Cord Mesenchymal Stem Cells; 16S rRNA se-quencing; Intestinal Flora.

Abstract

Neuroinflammation is a key factor leading to the occurrence of neurodegenerative diseases. Human Umbilical Cord Mesenchymal Stem Cells (hUC-MSCs) exert anti-inflammatory functions. However, the mechanism of the effect of hUC-MSCs therapy on the intestinal flora of neuroinflammatory models is still unclear. The purpose of this study is to explore the regulatory effect of hUC-MSCs on the intestinal flora of the LPS-induced neuroinflammation models. We used the hUC-MSCs and LPS-induced neuroinflammation mouse model as the research object. To explore the neuroprotective effect of hUC-MSCs on neuroinflammation models, behavioral tests, Nissl stain, Western Blot, 16S rRNA sequencing, and bioinformatics analysis were performed. We found that LPS suppressed the cognition and behavior of mice, but the treatment of hUC-MSCs could improve them, and hUC-MSCs inhibited LPS-induced neuronal death in the hippocampus and cortex. In addition, the results of Western Blot showed that hUC-MSCs could inhibit the activation of astrocytes and microglia and the expression of inflammatory factors. 16S rRNA sequencing showed that LPS induction reduced *Oscillospira* and *Odoribacter*, and increased *Prevotella*, *Coprococcus*, *Dialister*, *Veillionella,* and *Ruminnococcus*. This study indicated that hUC-MSCs may play a neuroprotective effect by regulating intestinal flora.

Introduction

Neuroinflammation is the main pathogenic factor of neurodegenerative diseases, which is closely related to the activation of astrocytes and microglia in the central nervous system [1,2]. Microglia and astrocytes can be activated by sensing external harmful substances or pro-inflammatory stimulus [3], leading to neuroinflammation, cognitive and behavioral dysfunction, and neuronal damage [4]. Therefore, modulating neuroinflammation is a potential therapeutic strategy for preventing/treating neuroinflammation-related diseases.

Lipopolysaccharide (LPS) is an endotoxin derived from gram-negative bacteria that is a strong stimulator of activation of microglia and astrocytes [5]. LPS can interact with Toll-Like Receptor 4 (TLR4) in microglia with triggering Nuclear Factor Kappa-B (NF-κB) and Mitogen-Activated Protein Kinase (MAPK) signaling pathways, thus inducing the secretion of pro-inflammatory factors [6]. The secretion of pro-inflammatory factors will promote activation of microglia and astrocytes further inducing neuron death, Blood-Brain Barrier (BBB) and gut barrier disruption, abnormal cognition and behavior, and imbalance of gut microbiota [7,8]. Therefore, the LPS-induced mouse models are used as a model of neuroinflammation.

Human Umbilical Cord Mesenchymal Stem Cells (hUC-MSCs) are characterized by high proliferation, multi-lineage differentiation potential, and immune regulation. It is known that hUC-MSCs can treat degenerative diseases through immunomodulation, paracrine, and regeneration effects [9]. In this study, we investigated the efficacy of hUC-MSCs in a mouse model of LPS-induced neuroinflammation. The results indicate hUC-MSCs administration may affect the gut microbiota and have a neuroprotective effect via immunomodulatory and brain-gut-microbiota axis, providing strong support for the use of hUC-MSCs as a uniform and sustainable source of cells for neuroinflammation-related diseases therapy.

Methods

Cultivation of hUC-MSCs

The hUC-MSCs (Cat. No.1163, Kangyanbao, China) were purchased from Kangyanbao (Beijing) Stem Cell Technology Co., Ltd (http://www.go007.com/zp/comp_10997163.html), and the isolation and extraction of this cell obtained ethical approval. The cells were cultured in a DMEM medium (BI, Israel), which contained 10% Fetal Bovine Serum (FBS, BI, Israel) and 100 U/mL penicillin (BI, Israel), and 100 μg/mL streptomycin (BI, Israel). The new medium was replaced with fresh medium every 2 days. When the confluency of the cells reached 80%-90%, the cultured cells were passaged with 0.25% trypsin (BI, Israel). The cells at passages 3-5 were used for the experiments.

Detection of surface markers

When hUC-MSCs reached 80-90% confluence, hUC-MSCs were harvested and prepared into a single cell suspension of 1×10⁶ cells, fixed with 4% paraformaldehyde (Solarbio, China), and washed with PBS. The cells were labeled with surface markers, including CD73 (FITC, BD Biosciences, San Jose, CA, USA), CD90 (FITC, BD Biosciences, San Jose, CA, USA), and CD105 (FITC, BD Biosciences, San Jose, CA, USA). The negative marker was a mixture of CD34, CD45, CD11b, CD19 and HLA-DR (PE, BD Biosciences, San Jose, CA, USA). Negative control (BD Biosciences, San Jose, CA, USA) and isotype control (BD Biosciences, San Jose, CA, USA) were used to calibrate the fluorescence intensity of the cells. The expression of surface markers on labeled cells was detected by flow cytometry (BD Biosciences, NJ).

Osteogenesis, adipogenesis, and chondrogenesis differentiation

For adipogenic differentiation, hUC-MSCs were seeded in a 6-well plate (Eppendorf, USA). After hUC-MSCs reached 100% confluence, the cell was cultured with an adipogenic differentiation medium (Cyagen Biosciences, China). hUC-MSCs in routine culture medium served as control. All mediums were changed twice per week for 3 weeks. Staining of hUC-MSCs was performed with Oil Red O (Cyagen Biosciences, China). For osteogenic induction, hUC-MSCs were cultured to a confluence of 60-70%. The supernatant was discarded, and an osteogenic differentiation medium (Cyagen Biosciences, China) was added. The osteogenic medium was changed every 3 days, and Alizarin Red (Cyagen Biosciences, China) staining was performed after 3 weeks of induction. For chondrogenic differentiation, 3-4×10⁵ cells were transferred to a 15 mL centrifuge tube, centrifuged at 250 g for 4 min to form a pellet. Chondrogenic induction complete medium (Cyagen Biosciences, China) was added. Finally, the cap of the centrifuge tube was loosened and placed in a 37°C, 5% CO_2 incubator. Change the culture medium every 2-3 days. With 21-28 days of continuous induction, the cartilage balls were fixed with paraformaldehyde and cut by a cryostat. And then the slice was stained with Alcian Blue (Cyagen Biosciences, China) and observed with a microscope.

LPS modeled

Derived from E. coli 055: B5, LPS (Sigma-Aldrich, L2880) was dissolved in 1 mL of normal saline to prepare a mother liquor of 10 mg/mL and stored in a refrigerator at -20°C. According to the injection dose of 0.5 mg/kg/day, the working solution was prepared, and the 0.22 μm filter was used for filtration and sterilization. Each mouse was injected with a 100 μL working solution of LPS for 5 days by intraperitoneal injection.

Animal and treatment

Twenty-one C57BL/6 mice (male, 6-8 weeks) were purchased from the Peking University School of Medicine. In a stable environment with constant temperature (25 ± 1°C) and relative humidity (55 ± 5%), all animals are kept in standard animal cages, having free access to feed and water. The procedures for the care and use of animals have been approved by the ethics committee of Peking University School of Medicine, and all applicable institutions and government regulations regarding the ethical use of animals have been complied with. The mice were randomly divided into 3 groups (n=7), including the control group, the LPS group (intraperitoneal injection of LPS 0.5 mg/kg for 5 days and tail intravenous injection of normal saline), and the LPS+hUC-MSCs group (It is abbreviated as hUC-MSCs in the article below), the hUC-MSCs group (1×10⁶ cells/mouse) was administered by tail vein injection 4 times at 1, 5, 9, 13 days, 0.5 mg/kg LPS was injected into each recipient mouse by intraperitoneal injection at 9-13 day in the hUC-MSCs group.

Behavioral experiment

Morris water maze (MWM)

MWM [10] was mainly used to evaluate the learning and memory abilities of mice. Each mouse was trained for 5 days. The platform was 1 cm above the water surface on the first day, and on the second to fifth days added white dye to the water and hide the platform 1cm below the water surface. Trained 3

times a day, the mice were put in different water points, and we recorded the time of the mice landing within 60 s. If a mouse didn't find the platform, we guided the mouse to the platform, where the mouse was allowed to sit for 10 s, and then we dried it with a paper towel and placed a heat lamp under it to dry before we put it in a cage. On the sixth day, the platform was removed. The staying time of the mouse in the target quadrant and the time passing through the platform were observed to evaluate the learning and memory ability of the mouse.

Novel object recognition test

Novel Object Recognition (NOR) test was also used to analyze the learning and memory abilities of mice [11]. On the first day, a mouse was stayed in an empty box for 10 minutes to adapt to the environment of the box. On the second day, two of Object A (cylinder) were placed in the box. A 10-min object familiarization phase was conducted. An hour later Object A was replaced by Object B (cylinder and cone), and a 6-min testing period was conducted. We observed the object recognition times. The novel object recognition ratio = time novel object/(time novel object + time old object) ×100%. Object exploration was defined when a rat directed its nose at an object within 2 cm or less and was actively investigating the object.

The pole test, wire hang test and rotarod test

A self-made wooden pole with a diameter of 1 cm and a height of 60 cm was placed in the home cage. The mouse was placed head upon the top of the rod, and the time that it took the mouse to fall from the top of the rod to the ground was recorded. The interval between each test is I min. As Kuribara's test method said that a metal wire is placed horizontally on both ends of the self-made plexiglass suspension test box, distancing 30 cm from the ground [12]. In the experiment, the mouse's front paws were suspended on the metal online. We checked the number of paws that the mouse could grasp on the main wire. The scoring standards range from 1 to 3 (zero= 1 points, one= 2 points, two= 3 points). The interval of each test is 1 min. The rotarod test requires animals to keep balance and move continuously on a roller, which is widely used to detect movement coordination [13]. The diameter of the roller is 6 cm, and the speed is 20 r/min. After each mouse was trained 5 times, the time that the mouse was on the roller was recorded. The interval of each test is 1 min. In the above test, high-speed cameras were used to record the behavioral effects of mice and were analyzed by people who were not involved in the experiment. All experiments were performed 3 times.

Tissue preparation

After the behavioral test was over, the mice were cut off from feeding for 12 h to facilitate obtaining materials. First, the mice were anesthetized to let the mice lose consciousness. Brain tissue was quickly placed in a -80 °C freezer after the addition of liquid nitrogen. After the tissue to be sliced was fixed in 4% paraformaldehyde for 24 h, dehydrated with 10% and 15% sucrose solution overnight in turn, and then soaked in 30% sucrose solution. After the tissue was completely sunk to the bottom in a 30% sucrose solution, the tissue samples were embedded in OCT (Sakura, China), stored at -80 °C.

Western blot

The brain tissue was lysed in 8 M urea (Xilong Scientific, China), centrifuged the lysis buffer mixture and collected the supernatant. The protein concentration was quantified by BCA

(Beyotime, China). The proteins were separated by 15% sodium dodecyl sulfate-polyacrylamide gel electrophoresis, transferred to PVDF membrane (Millipore), and incubated for 1 h at room temperature with 5% skimmed milk powder in PBST. Subsequently, the bands of specific protein molecular weights were cut out and combined with primary antibodies overnight at 4°C, including, IL-6 Mouse Monoclonal Antibody (Beyotime, China, AF0201, 1:1000), IL1B Rabbit Polyclonal Antibody (Beyotime, China, AF7209, 1:1000), TNF-α Rabbit Polyclonal Antibody (Beyotime, China, AF8208, 1:1000), GFAP Mouse Monoclonal Antibody (Beyotime, China, AF0156, 1:1000), Iba-1 Rabbit Polyclonal Antibody (Beyotime, China, AF7143, 1:1000) and β-Actin Mouse Monoclonal Antibody (Beyotime, China, AF5001, 1:1000). Then, the protein bands were washed with PBST 3 times for 10 min, incubated with the diluent of the HRP-labeled Goat Anti-Rabbit IgG(H+L) (Beyotime, China, A0208, 1:1000) or HRP-labeled Goat Anti-Mouse IgG(H+L) (Beyotime, China, A0216, 1:1000) at room temperature for 1 h. After being covered with the substrate, each protein band was visualized and recorded by a chemiluminometer (Shenhua Technology, China). The data were obtained using ImageJ analysis software.

Nissl stain

Washed by PBST, a 30 μm frozen section was fixed with 4% paraformaldehyde for 10 min, washed with distilled water for 2 min. Then the brain slice was stained with Nissl stain for 10 min and was washed twice with distilled water, and the brain slice was dehydrated with 95% ethanol for 2 min 2 times. We dropped xylene on the brain slice for 5 min twice to promote the transparency of the brain slice. The morphology of hippocampal neurons was observed under a microscope to get 5 pictures for each section.

16 S rRNA Sequencing

We used sterilized tweezers to collect 2-3 pieces of fresh feces from each mouse, putting them in the sample storage solution (n=3, Guhe, China). The DNA of samples was extracted, using nucleic acid extraction or purification reagents (GHFDE100, Guhe, China). The quantity and quality of DNA were determined by the NanoDrop ND-1000 spectrophotometer (Thermo Fisher Scientific, Waltham, MA, USA). We performed a quality inspection on the sample, selected one or several variant regions after passing the quality inspection, and designed universal primers for amplification. The configured PCR system performs PCR amplification according to the following reaction conditions: predenaturation at 98°C for 30 s, and the next 25 cycles: denaturation 98°C 15 s, annealing at 58°C 15 s, and extension at 72°C 15 s. The final extension is 72°C for 1 min. The PCR product was purified with AMPure XP Beads (Beckman Coulter, Indianapolis, IN) and quantified using PicoGreen dsDNA Assay Kit (Invitrogen, Carlsbad, CA, USA). After quantification, the Illlumina HiSeq4000 pair-end 2×150 bp platform was used for sequencing. The obtained sequencing data were used for species identification analysis.

Bioinformatics analysis

Based on the OTU clustering results and taxonomic information, we could further in-depth statistical analysis and visual analysis of community structure and phylogeny, and function prediction analysis. Sequence data analysis mainly uses QIIME and R package (v3.2.0). We used QIIME software to calculate the alpha diversity index. Beta diversity analysis was to calculate the UniFrac distance metric through Qimme software [14,15],

drawing PCA and PCoA diagrams to perform Beta diversity analysis on the microbial community structure of different samples.

The t-tests and the Monte Carlo permutation tests were used to draw box plots to compare the differences in Unifrac distances between groups. PERMANOVA (Permutational Multivariate Analysis of Variance) [15] was used to evaluate the markers of microbial community structure differentiation between groups, from the "vegan" of the R package. Taxonomic groups and abundance were visualized by MEGAN [16] and GraPhlAn [17]. The Venn diagram was generated based on the "VennDiagram" of the R package to visualize the common and unique OTUs between samples or groups. Kruskal method of the R stats package was used to compare the differences in phyla, class, order, family, and genus among samples or groups. LEfSe analysis used LEfSe default settings to detect differences in taxonomies between groups. Random forest analysis used the default settings of the R package's "random Forest" to compare differences between groups. Prediction of microbial function was based on the PICRUSt [18]. Metagenomic Profiles (STAMP, v2.1.3) [19] were used to further analyze the output files. The analysis of β diversity in species and function based on Meta-Storms distance was done with Parallel-META 3 (version 3.3.2).

Statistical analysis

All data in the article were presented as means ± SD from at least three independent experiments. For analysis of learning and cognitive abilities, neuronal death, and western blot, one one-way ANOVA was performed, and comparisons between two groups were processed with Student's t-test. The t-tests and the Monte Carlo permutation tests were used to draw box plots to compare the differences in Unifrac distances between groups in the 16 S rRNA Sequencing. $P<0.05$ was considered significant. ***$P < 0.001$; **$P < 0.01$; *$P < 0.05$.

Results

Morphological observation and identification of hUC-MSCs

Under the ordinary light microscope, the hUC-MSCs have a uniform fibrous morphology (Fig. 1a). There was no obvious change in cell morphology during cell proliferation. When hUC-MSCs were cultured in the osteogenic and the adipogenic induction medium for 21 days, small red lipid droplets could be found in the cytoplasm of cells after staining with Oil Red O (Fig. 1b), and many red nodules could be observed after staining with Alizarin Red (Fig. 1c). We added cartilage complete medium to hUC-MSCs for about 4 weeks, took out the cartilage, and stained the frozen section with Alcian blue. It was found that the cells produced blue glycosaminoglycans, which was an important raw material for the formation of articular cartilage tissue. So, this result showed that hUC-MSCs have formed cartilage (Fig. 1d). Overall, these results suggested that hUC-MSCs had the abilities of adipogenic differentiation, osteogenic differentiation, and chondrogenic differentiation. In addition, the surface marker identification results showed that the expression of negative markers (CD34, CD45, CD11b, CD19, and HLA-DR) were 0% in the experimental samples, and the expression levels of the positive markers, including CD73, CD90, and CD105, were 100%, 100% and 96.37%, respectively (Fig. 1e). To sum up, those results showed that hUC-MSCs extracted had a high proliferation capacity, multi-lineage differentiation potential, and stable immune phenotype of MSCs according to the International Society for Cell Therapy [20].
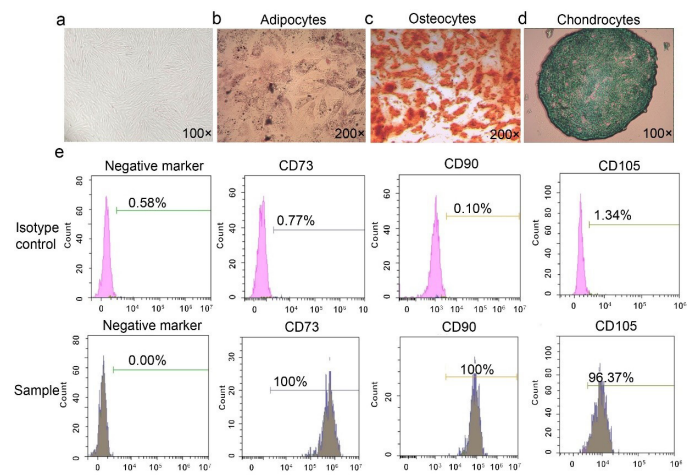
Figure 1: Morphological observation and identification of hUC-MSCs. **(a)** Morphological observation of hUC-MSCs under the ordinary light microscope. **(b)** Adipogenesis of hUC-MSCs stained with oil red O. **(c)** Osteogenesis image of hUC-MSCs induced by an osteogenic medium. **(d)** The frozen sections of cartilage balls of hUC-MSCs were stained with Alcian blue and were positive. **(e)** Flow cytometry to identify stem cell surface markers. The expression of negative markers (including CD34, CD45, CD11b, CD19, and HLA-DR) was 0.00%. The expression levels of the positive markers CD73, CD90, and CD105 were 100%, 96.37%, and 100%, respectively. hUC-MSCs: Human umbilical cord mesenchymal stem cells.

The hUC-MSCs could improve the learning and cognitive abilities in LPS-induced mice

We explored the effect of hUC-MSCs on the mouse models induced by LPS. The experimental flow chart was shown in Figure 2a. To evaluate the learning and cognitive ability of hUC-MSCs in LPS-induced mice, we conducted MWM and NOR tests. In the MWM test, we found significant differences in more precise and less precise time to plateau in the control group compared with the other two groups. In the behavioral trajectories of mice, target platform learning and memory abilities were investigated. We found that the swimming route of LPS-induced mice was tortuous, and the swimming route of hUC-MSCs-treated mice was simple (Figure 2b). It was also found that the residence time in the target quadrant of the LPS-induced mice was significantly reduced compared with the control group ($P < 0.01$), and the hUC-MSCs treatment group was significantly higher than the LPS-induced mice ($P < 0.001$, Figure 2c). Besides, the number of crossing the platform of LPS-inducted mice was significantly reduced compared with the control group ($P < 0.01$), and the hUC-MSCs treatment group had a significant improvement compared with the LPS group ($P < 0.01$, Figure 2d). Similarly, the results of the NOR test further showed that the new object recognition index of the LPS treatment group was significantly reduced ($P < 0.001$), but the treatment of hUC-MSCs significantly increased the new object recognition index ($P < 0.01$, Figure 2e). So, we concluded that the treatment of hUC-MSCs could improve the learning and cognitive abilities of the LPS-induced mice.
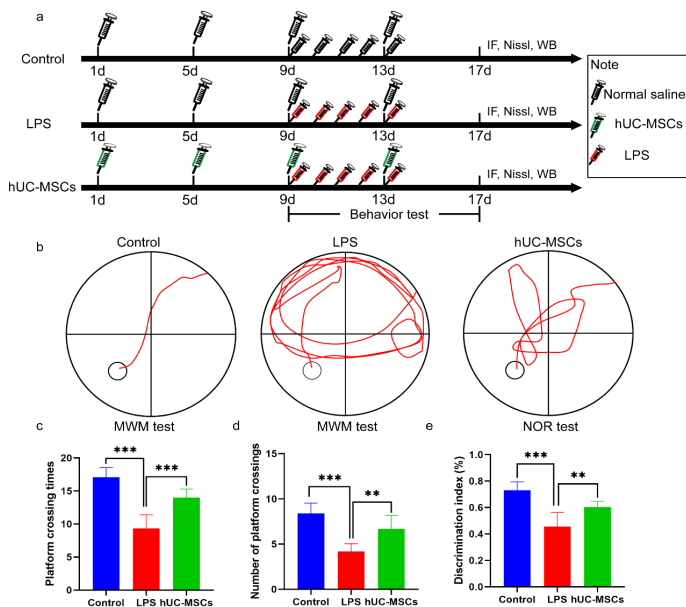
Figure 2: The learning and cognitive functions of LPS-induced mice were improved by hUC-MSCs (n=7). **(a)** Schematic diagram of the experimental process. The black syringe represents the injection of the same amount of normal saline, and the green syringe represents the injection of hUC-MSCs. In the MWM test, **(b)** Mouse behavior trajectory on the 5th day. **(c)** Platform crossing times. **(d)** Numbers of platform crossings. **(e)** The new object recognition index in the NOR test. The experimental data in the figure are presented in the form of means ± SD; P-value was calculated with ANOVA analysis. ***P < 0.001; **P < 0.01; *P < 0.05. Control group: the health mice; LPS group: the LPS-induced mice; hUC-MSCs group: the LPS-induced mice with hUC-MSCs treatment. MWM: Morris Water Maze; NOR: Novel Object Recognition.
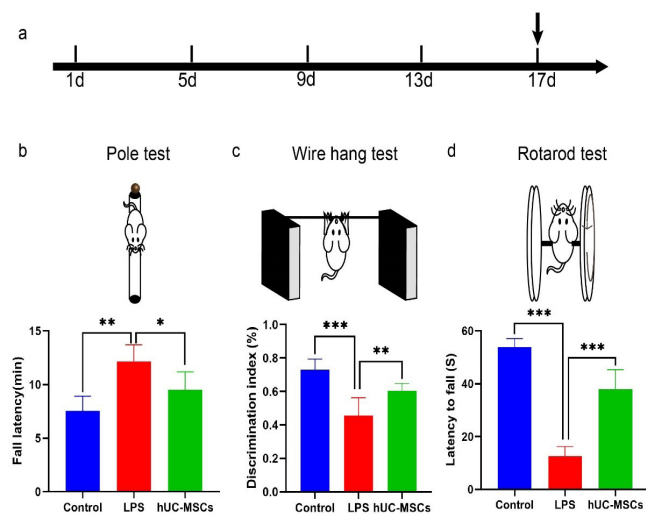
Figure 3: Behavioral disorders improvement with the hUC-MSCs treatment (n=7). **(a)** Behavioral test time point. **(b)** Pole test. **(c)** Wire hang test. **(d)** Rotarod test. The experimental data in the figure are presented in the form of means ± SD; P-value was calculated with ANOVA analysis. ***P < 0.001; **P < 0.01; *P < 0.05.

The hUC-MSCs abrogated motor deficits in LPS-induced neuroinflammatory mice models

To explore the influence of hUC-MSCs on the motor behavior of LPS-induced neuroinflammation models, we conducted a pole test, wire hang test, and rotarod test. The test time was arranged on the 17th day of the experiment (Figure 3a). In the

pole test, compared with the LPS group, the time of mouse falling from the top of the rood to the ground in the control group was significantly low and the hUC-MSCs treatment group was lower than the LPS group in latency to fall (P < 0.05, Figure 3b). In the wire hang test, compared with the LPS group, the scores of the control group and the hUC-MSCs treatment group was significantly different, which meant that an improved grip by hUC-MSCs treatment was detected as a higher score in the wire hang test than the LPS group (P < 0.001, Figure 3c). Meanwhile, the longer time of mice staying on the rotating rod, the stronger the coordination ability of mice in the rotarod test. Compared with the LPS group, the treatment of the hUC-MSCs group extremely increased the residence time of LPS-induced mice (P < 0.001, Figure 3d). The results showed that hUC-MSCs treatment could improve behavioral disorders in the LPS-induced mice.

The hUC-MSCs inhibited LPS-induced neuronal death

To explore the survival state of neurons, we performed a Nissl stain to observe the distribution and number of neurons in the hippocampus, CD3 area, and cortex. Compared with the control group, the number of stained neurons in the LPS group was smaller and the staining color was lighter, indicating that there were fewer Nissl bodies in the cell. Compared with the LPS group, the hUC-MSCs group has more neurons and darker staining of neurons, indicating that the number of intracellular Nissl bodies was larger and the neuronal cells were good (Figure 4a). To further count the number of neurons in different parts, we used ImageJ to count the area ratio of neurons and the number of neurons. In the hippocampus, the proportion of neurons in the LPS group is lower than that in the control group (P < 0.01), and hUC-MSCs could increase the proportion of neurons (Figure 4b, P < 0.001). In addition, the number of neurons in the CD3 area (Figure 4c) and cortex (Figure 4d) was significantly lower in the LPS group than in the control group, and the number of neurons in the hUC-MSCs group was higher than that in the LPS group. In short, these results indicated that LPS promoted the loss of neurons, and the treatment of hUC-MSCs provided neuroprotective effects in the brain.
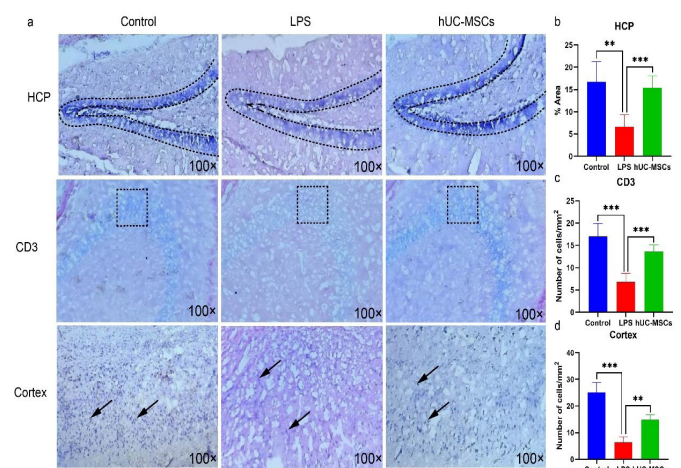
Figure 4: Pictures of Nissl stain (n=3). **(a)** Stained images of neurons in the hippocampal dentate gyrus, CD3, and cortex. **(b)** A statistical picture of the area ratio of neurons in the cortex. **(c)** The number of neurons in CD3. **(d)** The number of neurons in the cortex. The experimental data in the figure are presented in the form of means ± SD; P-value was calculated with ANOVA analysis. ***P < 0.001; **P < 0.01; *P < 0.05. HCP: the hippocampus.

The hUC-MSCs inhibited activation of microglia and astrocytes and expression of pro-inflammatory cytokines

To evaluate the neuroprotective effect of hUC-MSCs, we used western blot to detect the expression level of inflammatory factors in the brain, including IL-6, IL1B, TNF-α, Iba-1 and GFAP. We found that inflammatory factors, Iba-1 and GFAP in the LPS mice were highly expressed, and the expression was decreased after hUC-MSCs treatment (Figure 5a). The expression of IL-6, IL1B and TNF-α were decreased in LPS-induced mice, and were increased under the treatment of hUC-MSCs (Figure 5b). These results demonstrated that treatment with hUC-MSCs improved LPS-induced neuroinflammation.
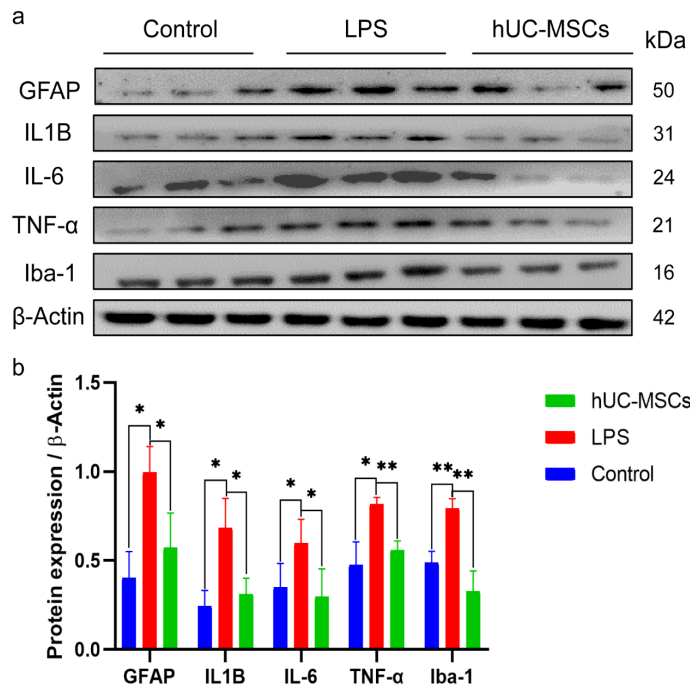
Figure 5: Expression of neuroinflammatory factors (n=3). **(a)** Representative western blot immunolabeling of GFAP, Iba-1, IL1B, TNF-α, and IL-6. **(b)** Protein expression/β-Actin of GFAP, Iba-1 and IL1B, TNF-α and IL-6. The experimental data in the figure are presented in the form of means ± SD; P-value was calculated with ANOVA analysis. ***P < 0.001; **P < 0.01; *P < 0.05.

The hUC-MSCs reversed the reduction of gut microbial diversity and richness in LPS-induced mice

To explore the effects of inflammation and stem cell therapy on the gut microbiota, we performed 16S rRNA sequencing and analyzed the Alpha and Beta diversity analysis of gut microbes. Shannon, Simpson, and Chao1 indexes were three important indexes that reflect the diversity of Alpha. Generally speaking, the Shannon index was larger, and the species richness was higher. Compared with the other two groups, we found that the Shannon index of the control group was the lowest. It was worth mentioning that the abundance of the hUC-MSCs group was increased, compared with the LPS group (Figure 6a). Contrary to the Shannon index, when the Simpson index value was big, the community diversity was low. The control group had the highest community diversity and the LPS group had the lowest community diversity (Figure 6b). Chao1 index was used to estimate the diversity of microorganisms. Like the Shannon index, the Chao1 index was bigger, community diversity was higher. Here we found that compared with the LPS group, the gut microbial diversity of the normal group was reduced, while the gut microbial diversity of the hUC-MSCs treatment was significantly

increased, even it was higher than the control group (Figure 6c). The above results indicated that the hUC-MSCs improved the decline in the diversity of gut microbes in the LPS-induced mice. Multivariate statistical methods principal component analysis (PCA, Principal Component Analysis) and principal coordinate analysis (PCoA, Principal) were other analysis dimension that reflects biodiversity. The PCA results showed that the LPS group deviated greatly from the control group because the 3 points of the LPS group were not in the circle of the control group. Compared with the LPS group, the hUC-MSCs treatment group deviated significantly, and the hUC-MSCs treatment group was closer to the control group (Figure 6d). To explore the similarities and differences in the evolution of intestinal flora in different groups of mice, we conducted a PCoA analysis. The results revealed distinct microbiota composition clustering among control, LPS and hUC-MSCs groups, indicating that hUC-MSCs altered the gut microbiota, and hUC-MSCs treatment influences the microbiota composition significantly (Figure 6e). In summary, the intervention of hUC-MSCs improved the diversity and richness of the intestinal flora of LPS-induced mice to a certain extent.
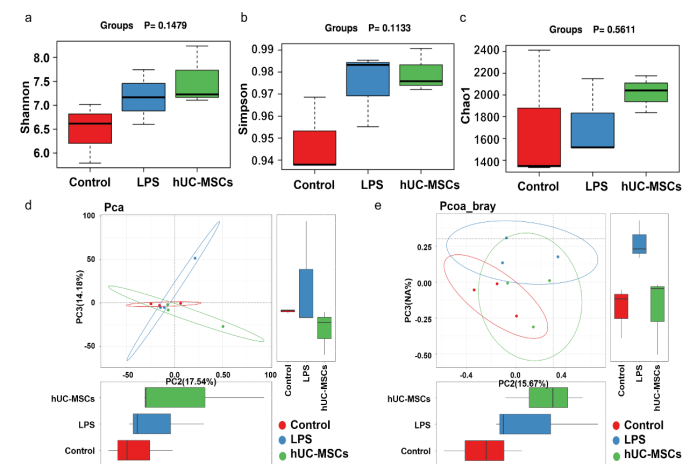
Figure 6: 16S rRNA sequencing and analysis results (n=3). **(a)** Shannon index. **(b)** Simpson index. **(c)** Chao1 index. **(d)** Principal Component Analysis (PCA, Principal Component Analysis). **(e)** Principal Coordinate Analysis (PCoA, Principal). Each dot represents a mouse and each circle represents a group. The experimental data in the figure are presented in the form of means ± SD; P-value was calculated with t-tests and the Monte Carlo permutation tests. ***P < 0.001; **P < 0.01; *P < 0.05.

The hUC-MSCs reduced the abundance of pro-inflammatory bacteria

To find different groups of different flora, we first analyzed the intestinal microbial differences between different groups at the genus level. The study found that there were obvious differences in *Oscillospira, Prevotella, Odoribacter*, *Coprococcus*, and *Ruminnococcu*, and other bacterial species. Studies have shown that compared with healthy patients, the abundance of *Oscillospira* in PD patients has increased [10]. Consistent with the results of this study, we found that the relative abundance of *Oscillospira* in the LPS treatment group was higher than that in the control group, while the abundance of *Oscillospira* in the hUC-MSCs treatment group was decreased. *Coprococcus* is also a kind of beneficial bacteria. In this study, we found that the *Coprococcus* richness of the hUC-MSCs treatment group was higher than that of the LPS induction group (Figure 7a). In order to select the difference markers, we performed LEfSe analysis, which showed that there are obvious difference markers be-

tween the LPS group and other groups, and the main difference was the difference in bacteria (Figure 7b). We also conducted a heat map analysis between groups based on the genus level and found that there was a clear trend in *Dialister* and *Veillionella*. LPS enhanced the expression of *Dialister* and *Veillionella* (Figure 7c). In addition, we also used the sample community distribution map of the species evolution tree to analyze the dominant species between different groups (Figure7d). The interrelationship between microorganisms meant the interrelationship between *Cyaobactcria, Bactcroidctcs, Vcrrucomicrobia,* and *Actinobactcria* (Figure 7d).
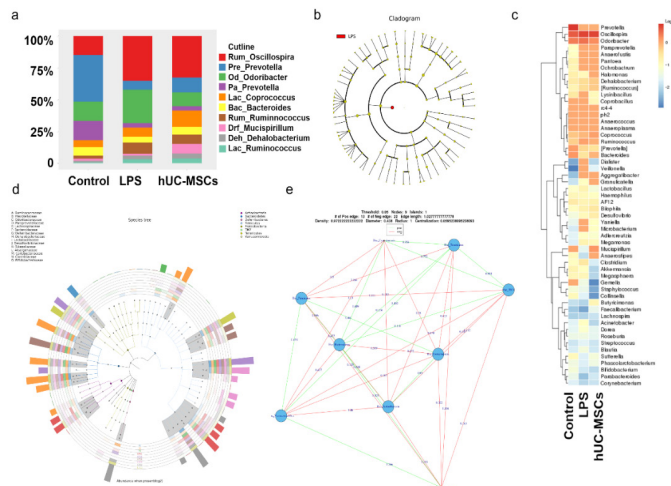
Figure 7: LPS-induced differences in the bacterial flora of mice. **(a)** A rich map of species composition between groups, taking the genus level as an example. **(b)** Out_formant. cladogram. **(c)** Thermal map analysis non_norm_100log10. **(d)** Graphlan, different color branches represent different classes (the legend in the upper right corner), in which the values of the heat map and the histogram are the original scale × 10000 after $\log_2$ conversion. **(e)** Phylum_networkand the node is larger, and the richness is higher. The green line indicates a positive correlation, and the red line indicates a negative correlation.

Discussion

Multiple intraperitoneal injections of LPS are the primary method for inducing neuroinflammation in mouse models [21,22], and LPS injections alter the composition of healthy gut microbiota. In the present study, we found that hUC-MSCs ameliorated LPS-induced cognitive deficits and behavioral impairments. Meanwhile, hUC-MSCs transplantation suppressed neuronal death in the hippocampus and the expression of inflammatory factors in the mouse brain, and improved gut microbiota composition in LPS-induced neuroinflammation mouse models. This study provides some data support for exploring the therapeutic mechanism of hUC-MSCs for neuroinflammation and neurodegenerative diseases and explaining the connection between stem cells, microorganisms and neuroinflammation.

It has been previously reported that hUC-MSCs transplantation has anti-inflammatory and neuroprotective effects in a microbead induced ocular hypertension rat model [23,24], and another study showed that hUC-MSCs regulate intestinal microorganisms in a rodent model of PD [25]. This provides some theoretical support for our experimental research. 3 times injections of hUC-MSCs before LPS induction was performed in this study. One reason is that MSCs are alive and have no specific targets. Studies suggest that MSCs can exert a wide range of effects in various aspects of disease, such as changing the microenvironment, enhancing cell activity, and immune regula-

tion [26,27]. This also means that MSCs do not achieve strong unique therapeutic effects, especially in small doses. Stem cell secretion changes in response to the microenvironment for survival. In addition, the harsh blood environment can lead to massive cell death. Strictly speaking, inflammation is a chronic injury. Stem cell pre-treatment helps to improve the microenvironment slowly, avoiding the generation of side effects such as factor storm and shock in the clinic [28]. Therefore, our experimental design is mainly focused on increasing the total dose administered to improve cell survival. On the other hand, stem cells are able to gradually adapt and respond to changes in the systemic environment upon LPS treatment, which is beneficial for relatively prolonged access to the secretory response of stem cells, improving the blood microenvironment [29].

In LPS-induced mice, the MWM test and NOR test were performed, which are used to assess learning and memory abilities [30]. The pole test, wire hang test, and rotarod test were used to evaluate the limb movement and coordination ability of mice [31,32]. Studies have shown that AD and PD are mainly caused by neuroinflammation [33,34]. In addition, the research found that Bone Marrow-Derived Mesenchymal Stem Cells (BM-MSCs) improved the cognitive impairment of AD mice [35], and one study reported that hUC-MSCs affect behavioral disorders and mobility in a rat of advanced PD model [36]. Our experimental results suggested that hUC-MSCs improved cognitive and behavioral impairments in a neuroinflammation model. It implied that hUC-MSCs may improve cognitive or behavioral impairments in AD or PD by affecting neuroinflammation.

Recent studies have shown that neuroinflammation leaded to changes in the gut microbiota [37], and hUC-MSCs have a certain effect on the ecological balance of intestinal flora [38]. Indeed, there is currently no reported direct evidence to explain how stem cells affect the gut microbiota. In our study, the intravenously injected stem cells did not come into direct contact with the gut, and there was no spatial intersection between them. However, our results identified changes in the microbiota in cell therapy strategies. In previous reports, changes in the gut microbiota were easily explained because the drug was absorbed by the gut and administered by gavage [39,40]. Therefore, we agreed that the mechanism after reading a lot of literature and having heated discussions, and the mechanism of hUC-MSCs how to affect the microbiota can be summarized into two points: the brain-gut axis and immune regulation.

In short, paracrine and endocrine plays a crucial role between MSCs, microbiota and neuroinflammation [41,42]. Although there is no spatiotemporal intersection between stem cells and gut tissue, several pathways can link hUC-MSCs, microbiota and neuroinflammation. On the one hand, hUC-MSCs that cross the blood-brain barrier alter the intracerebral microenvironment and influence the response of the gut microbiota through the vagus plexus [43]. we found that a variety of harmful bacteria were up-regulated in neuroinflammation but decreased in the cell therapy group, such as *Oscillospira* and *Odoribacter*, and we found that multiple probiotics were up-regulated in response to cell therapy, including *Prevotella*, *Coprococcus* and *Ruminnococcus*. Some researchers found *Oscillospira* was a key regulator of the colony in the related nervous syste [44], and the aggressive treatment reduces the composition of the Oscillospira microbial colony [45]. Previous studies have confirmed that *Coprococcus* and *Bacteroides* has anti-inflammatory and neuroprotective effects [28, 46-48]. Our findings are consistent with the microbiota changes of these studies. On the other hand,

stem cells injected into the blood after intravenous injection can improve the immune microenvironment of the blood, leading to endocrine changes, which in turn trigger the response of the intestinal flora[43]. LPS secretes pro-inflammatory cytokines by activating NF-κB and STAT1 pathways. The secretion of these inflammatory factors can trigger the inflammatory response of astrocytes and microglia in the brain [49], release more inflammatory factors, aggravate the inflammatory response of the brain, and lead to neuronal damage [50]. Studies have found that MSCs can modulate glial cells in neurodegenerative diseases *in vivo* and *in vitro* [51,52]. However, our work only supports that hUC-MSCs are neuroprotective and alter gut microbiota, but we do not clear the detailed mechanism of the effect, so further work is needed to explore.

Conclusions

In conclusion, this study found beneficial effects of hUC-MSCs transplantation in a model of LPS-induced neuroinflammation, and the hUC-MSCs transplantation can not only improve learning and cognitive ability but also improve behavioral disorders in the LPS model. The treatment of hUC-MSCs inhibited the activation of microglia and astrocytes, reduced the expression of pro-inflammatory cytokines, and inhibited neuronal death in the hippocampus. 16S rRNA sequencing showed that LPS changed the number and relative abundance of intestinal flora, especially for *Oscillospira* and *Coprococcus*, which were closely related to the occurrence of inflammation. This study suggested that the mechanism of hUC-MSCs how to affect the microbiota can be summarized into two points: the brain-gut axis and immune regulation. This discovery provided a potential treatment for preventing and delaying the development of neuroinflammation.

Consent for publication: Not applicable.

Ethics approval and consent to participate: Animal experimental procedures obtained approval from the Ethics Committees of Peking University School of Medicine.

Competing interests: The authors declare that they have no competing interests.

References

1. Kwon HS, Koh SH. Neuroinflammation in neurodegenerative disorders: The roles of microglia and astrocytes. Transl Neurodegener. 2020; 9: 42.

2. Kempuraj D, Thangavel R, Kempuraj DD, Ahmed ME, Selvakumar GP, et al. Neuro-protective effects of flavone luteolin in neuroinflammation and neurotrauma. Biofac-tors. 2021. 47: 190-197.

3. Park T, Chen H, Kevala K, Lee JW, Kim HY. N-Docosahexaenoylethanolamine ame-liorates LPS-induced neuroinflammation via cAMP/PKA-dependent signaling. Journal of neuroinflammation. 2016; 13: 284-284.

4. Andy SN, Pandy V, Alias Z, Kadir HA. Deoxyelephantopin ameliorates Lipopolysac-charides (LPS)-induced memory impairments in rats: Evidence for its anti-neuroinflammatory properties. Life Sci. 2018; 206: 45-60.

5. Xu J, Yuan C, Wang G, Luo J, Ma H, et al. Urolithins Attenuate LPS-Induced Neu-roinflammation in BV2Microglia via MAPK, Akt, and NF-κB Signaling Pathways. J Agric Food Chem. 2018; 66: 571-580.

6. Muhammad T, Ikram M, Ullah R, Rehman SU, Kim MO. Hesperetin, a Citrus Flavo-noid, Attenuates LPS-Induced Neuroinflammation, Apoptosis and Memory Impairments by Modulating TLR4/NF-κB Signaling. Nutrients. 2019; 11.

7. Rajendran L, Paolicelli RC. Microglia-Mediated Synapse Loss in Alzheimer's Disease. Journal of Neuroscience the Official Journal of the Society for Neuroscience. 2018; 38: 2911.

8. Tan W, Zhang Q, Dong Z, Yan Y, Fu Y, et al. Phosphatidylcholine Ameliorates LPS-Induced Systemic Inflammation and Cognitive Impairments via Mediating the Gut-Brain Axis Balance. Journal of Agricultural and Food Chemistry. 2020; 68: 14884-14895.

9. Lo Furno D, Mannino G, Giuffrida R. Functional role of mesenchymal stem cells in the treatment of chronic neurodegenerative diseases. J Cell Physiol. 2018; 233: 3982-3999.

10. Morris, R. Developments of a water-maze procedure for studying spatial learning in the rat. J Neurosci Methods. 1984; 11: 47-60.

11. Morrone CD, Bazzigaluppi P, Beckett TL, Hill ME, Koletar MM, et al. Regional dif-ferences in Alzheimer's disease pathology confound behavioural rescue after amyloid-β attenuation. Brain : A journal of neurology. 2020; 143: 359-373.

12. Zhang B, Wang PP, Hu KL, Li LN, Yu X, et al. Antidepressant-Like Effect and Mechanism of Action of Honokiol on the Mouse Lipopolysaccharide (LPS) Depression Model. Molecules. 2019; 24.

13. Mersmann N, Tkachev D, Jelinek R, Röth PT, Möbius W, et al. Aspartoacylase-lacZ knockin mice: an engineered model of Canavan disease. PLoS one. 2011; 6: e20336.

14. Lozupone C, Knight R. UniFrac: A new phylogenetic method for comparing micro-bial communities. Appl Environ Microbiol. 2005; 71: 8228-8235.

15. Lozupone CA, Hamady M, Kelley ST, Knight R. Quantitative and qualitative beta diversity measures lead to different insights into factors that structure microbial commu-nities. Appl Environ Microbiol. 2007; 73: 1576-1585.

16. Huson DH, Mitra S, Ruscheweyh HJ, Weber N, Schuster SC. Integrative analysis of environmental sequences using MEGAN4. Genome Res. 2011; 21: 1552-1560.

17. Asnicar F, Weingart G, Tickle TL, Huttenhower C, Segata N. Compact graphical representation of phylogenetic data and metadata with GraPhlAn. PeerJ. 2015; 3: e1029.

18. Langille MG, Zaneveld J, Caporaso JG, McDonald D, Knights D, et al. Predictive functional profiling of microbial communities using 16S rRNA marker gene sequences. Nat Biotechnol. 2013; 31: 814-821.

19. Parks DH, Tyson GW, Hugenholtz P, Beiko RG. STAMP: Statistical Analysis of Taxonomic And Functional Profiles. Bioinformatics. 2014; 30: 3123-3124.

20. Dominici M, Le Blanc K, Mueller I, Slaper-Cortenbach I, Marini F, et al. Minimal criteria for defining multipotent mesenchymal stromal cells. The International Society for Cellular Therapy position statement. Cytotherapy. 2006; 8: 315-317.

21. Czapski GA, Gajkowska B, Strosznajder JB. Systemic administration of lipopoly-saccharide induces molecular and morphological alterations in the hippocampus. Brain Res. 2010; 1356: 85-94.

22. Catorce MN, Gevorkian G. LPS-induced Murine Neuroinflammation Model: Main Features and Suitability for Pre-clinical Assessment of Nutraceuticals. Current neuro-pharmacology. 2016; 14: 155-164.

23. Ji S, Lin S, Chen J, Huang X, Wei C, et al. Neuroprotection of Transplanting Human Umbilical Cord Mesenchymal Stem Cells in a Microbead Induced Ocular Hypertension Rat Model. Curr Eye Res. 2018; 43: 810-820.

24. Ji S, Xiao J, Liu J, Tang S. Human Umbilical Cord Mesenchymal Stem Cells Attenu-ate Ocular Hypertension-Induced Retinal Neuroinflammation via Toll-Like Receptor 4 Pathway. Stem Cells Int. 2019; 9274585.

25. Sun Z, Gu P, Xu H, Zhao W, Zhou Y, et al. Human Umbilical Cord Mesenchymal Stem Cells Improve Locomotor Function in Parkinson's Disease Mouse Model Through Regulating Intestinal Microorganisms. Front Cell Dev Biol. 2021; 9: 808905.

26. Hoogduijn MJ, Popp F, Verbeek R, Masoodi M, Nicolaou A, et al. The immuno-modulatory properties of mesenchymal stem cells and their use for immunotherapy. Int Immunopharmacol. 2010; 10: 1496-1500.

27. Tsubokawa T, Yagi K, Nakanishi C, Zuka M, Nohara A, et al. Impact of anti-apoptotic and anti-oxidative effects of bone marrow mesenchymal stem cells with tran-sient overexpression of heme oxygenase-1 on myocardial ischemia. Am J Physiol Heart Circ Physiol. 2010; 298: H1320-1329.

28. Tan H, Zhao J, Zhang H, Zhai Q, Chen W. Novel strains of Bacteroides fragilis and Bacteroides ovatus alleviate the LPS-induced inflammation in mice. Appl Microbiol Biotechnol. 2019; 103: 2353-2365.

29. Nam Y, Yoon D, Hong J, Kim MS, Lee TY, et al. Therapeutic Effects of Human Mesenchymal Stem Cells in a Mouse Model of Cerebellar Ataxia with Neuroinflamma-tion. J Clin Med. 2020; 9.

30. Lissner LJ, Wartchow KM, Toniazzo AP, Gonçalves CA, Rodrigues L. Object recognition and Morris water maze to detect cognitive impairment from mild hippocam-pal damage in rats: A reflection based on the literature and experience. Pharmacol Bio-chem Behav. 2021; 210: 173273.

31. Wei P, Wang K, Luo C, Huang Y, Misilimu D, et al. Cordycepin confers long-term neuroprotection via inhibiting neutrophil infiltration and neuroinflammation after trau-matic brain injury. J Neuroinflammation. 2021; 18: 137.

32. Rui W, Li S, Xiao H, Xiao M, Shi J. Baicalein Attenuates Neuroinflammation by Inhibiting NLRP3/caspase-1/GSDMD Pathway in MPTP Induced Mice Model of Parkin-son's Disease. Int J Neuropsychopharmacol. 2020; 23: 762-773.

33. Leng F, Edison P. Neuroinflammation and microglial activation in Alzheimer dis-ease: Where do we go from here?. Nat Rev Neurol. 2021; 17: 157-172.

34. Hirsch EC, Standaert DG. Ten Unsolved Questions About Neuroinflammation in Parkinson's Disease. Mov Disord. 2021; 36: 16-24.

35. Nakano M, Kubota K, Kobayashi E, Chikenji TS, Saito Y, et al. Bone marrow-derived mesenchymal stem cells improve cognitive impairment in an Alzheimer's dis-ease model by increasing the expression of microRNA-146a in hippocampus. Sci Rep. 2020; 10: 10772.

36. Wang Z, Chen A, Yan S, Li C. Study of differentiated human umbilical cord-derived mesenchymal stem cells transplantation on rat model of advanced parkinsonism. Cell Biochem Funct. 2016; 34: 387-393.

37. Zhao Z, Ning J, Bao X, Shang M, Ma J, et al. Fecal microbiota transplantation pro-tects rotenone-induced Parkinson's disease mice via suppressing inflammation mediated by the lipopoly-saccharide-TLR4 signaling pathway through the microbiota-gut-brain axis. Microbiome. 2021; 9: 226.

38. Li Y, Shi G, Han Y, Shang H, Li H, et al. Therapeutic potential of human umbilical cord mesenchymal stem cells on aortic atherosclerotic plaque in a high-fat diet rabbit model. Stem Cell Res Ther. 2021; 12: 407.

39. Wang X, Sun G, Feng T, Zhang J, Huang X, et al. Sodium oligomannate therapeuti-cally remodels gut microbiota and suppresses gut bacterial amino acids-shaped neuroin-flammation to inhibit Alzheimer's disease progression. Cell Res. 2019; 29: 787-803.

40. Kaur H, Nagamoto-Combs K, Golovko S, Golovko MY, Klug MG, et al. Probiotics ameliorate intestinal pathophysiology in a mouse model of Alzheimer's disease. Neuro-biol Aging. 2020; 92: 114-134.

41. Bonsack B, Corey S, Shear A, Heyck M, Cozene B, et al. Mesenchymal stem cell therapy alleviates the neuroinflammation associated with acquired brain injury. CNS Neurosci Ther. 2020; 26: 603-615.

42. Dabrowska S, Andrzejewska A, Lukomska B, Janowski, M. Neuroinflammation as a target for treatment of stroke using mesenchymal stem cells and extracellular vesicles. J Neuroinflammation. 2019; 16: 178.

43. Leclair-Visonneau L, Neunlist M, Derkinderen P, Lebouvier T. The gut in Parkin-son's disease: Bottom-up, top-down, or neither?. Neurogastroenterol Motil. 2020; 32: e13777.

44. Petrov VA, Saltykova IV, Zhukova IA, Alifirova VM, Zhukova NG, et al. Analysis of Gut Microbiota in Patients with Parkinson's Disease. Bull Exp Biol Med. 2017; 162: 734-737.

45. Chen R, Wu P, Cai Z, Fang Y, Zhou H, et al. Puerariae Lobatae Radix with huanxiong Rhizoma for treatment of cerebral ischemic stroke by remodeling gut micro-biota to regulate the brain-gut barriers. J Nutr Biochem. 2019; 65: 101-114.

46. Valles-Colomer M, Falony G, Darzi Y, Tigchelaar EF, Wang J, et al. The neuroactive potential of the human gut microbiota in quality of life and depression. Nat Microbiol. 2019; 4: 623-632.

47. Vascellari S, Palmas V, Melis M, Pisanu S, Cusano R, et al. Gut Microbiota and Metabolome Alterations Associated with Parkinson's Disease. mSystems. 2020; 5.

48. Keshavarzian A, Green SJ, Engen PA, Voigt RM, Naqib A, et al. Colonic bacterial composition in Parkinson's disease. Mov Disord. 2015; 30: 1351-1360.

49. Liddelow SA, Guttenplan KA, Clarke LE, Bennett FC, Bohlen CJ, et al. Neurotoxic reactive astrocytes are induced by activated microglia. Nature. 2017; 541: 481-487.

50. Orihuela R, McPherson CA, Harry GJ. Microglial M1/M2 polarization and metabolic states. Br J Pharmacol. 2016; 173: 649-665.

51. Kim S, Kim YE, Hong S, Kim KT, Sung DK, et al. Reactive microglia and astrocytes in neonatal intraventricular hemorrhage model are blocked by mesenchymal stem cells. Glia. 2020; 68: 178-192.

52. Sun H, Bénardais K, Stanslowsky N, Thau-Habermann N, Hensel N, et al. Therapeu-tic potential of mesenchymal stromal cells and MSC conditioned medium in Amyo-trophic Lateral Sclerosis (ALS)- in vitro evidence from primary motor neuron cultures, NSC-34 cells, astrocytes and microglia. PloS one. 2013; 8: e72926.